INDERSCIENCE PUBLISHERS
Linking academia, business and industry through research

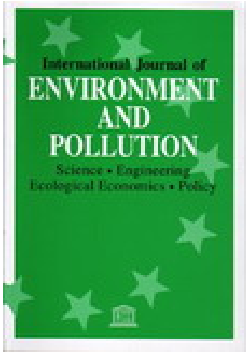

International Journal of Environment and Pollution

ISSN online: 1741-5101 - ISSN print: 0957-4352
https://www.inderscience.com/ijep

Marginal emission reduction costs of regional energy system transformation enabled by digital economy from the perspective of supply chain

Wenjuan Liu, Wenbo Ma

DOI: 10.1504/IJEP.2026.10078072

Article History:

Received:	05 September 2025
Last revised:	06 March 2026
Accepted:	01 April 2026
Published online:	04 September 2026

Marginal emission reduction costs of regional energy system transformation enabled by digital economy from the perspective of supply chain

Wenjuan Liu

College of Economics and Management,
Henan Polytechnic,
Zhengzhou, 450046, Henan, China
Email: 33010@hnzj.edu.cn

Wenbo Ma*

College of Business Administration,
Zhejiang University of Finance and Economics Dongfang College,
Haining, 314408, Zhejiang, China
Email: 20131016@zufedfc.edu.cn
*Corresponding author

Abstract: The existing supply chain management model cannot effectively control unit-level marginal emission-reduction costs. This paper constructs a multi-level, integrated framework based on the extreme gradient boosting (XGBoost) algorithm to capture the nonlinear relationships among electricity prices, weather, industrial activities, and historical loads, and to output node loads and carbon-emission boundaries dynamically. The prediction results are transmitted to the mixed-integer linear programming (MILP) model in real time, which optimises the carbon-emission path using piecewise linear control and global constraints to minimise the unit marginal emission-reduction cost. The node carbon emission data is written to the Hyperledger Fabric blockchain after encryption, enabling full-link, end-to-end encrypted evidence storage and traceability. Experiments show that when the carbon quota is set to 50% of the system's baseline emissions, the unit marginal emission-reduction cost is reduced from 278 yuan/ton to 245 yuan/ton.

Keywords: digital economy integration; marginal abatement cost; regional energy system; supply chain coordination; carbon information governance.

Reference to this paper should be made as follows: Liu, W. and Ma, W. (2026) 'Marginal emission reduction costs of regional energy system transformation enabled by digital economy from the perspective of supply chain', *Int. J. Environment and Pollution*, Vol. 76, No. 8, pp.1–26.

Biographical notes: Wenjuan Liu is an Associate Professor in Henan Polytechnic. She obtained her Master's degree from the University of Electronic Science and Technology of China. Her main research direction is accounting.

Wenbo Ma is currently employed at Zhejiang University of Finance and Economics Dongfang College, majoring in Marketing, and holds the title of Lecturer. He studied in the USA for three years and obtained a Master of

Business Administration degree. The main research directions are management, marketing, service marketing, education, behavioural economics, industrial economics and other fields.

1 Introduction

With the advancement of the ‘dual carbon’ goals, the regional energy system is transforming from a traditional centralised structure to a low-carbon system with multi-energy complementarity and coordinated dispatch. This process not only depends on the increase in the penetration rate of clean energy but is also subject to the collaborative efficiency and carbon emission control capabilities of each link in the supply chain (Kong et al., 2025; Shan-Shan et al., 2023). The development of the digital economy has provided a new technical foundation for refined scheduling, transparent information transmission, and multi-agent collaboration in regional energy systems, especially with strong regulatory potential for data-driven, platform-based collaboration and smart contract execution (Shahbaz et al., 2022; Wang et al., 2022). In this context, promoting the deep integration of the digital economy and the regional energy supply chain, and building an efficient, transparent, and low-cost mechanism for carbon emission reduction are of key significance for improving the transformation efficiency of the regional energy system (Coors and Padsala, 2024; Gu et al., 2025).

There are still many technical bottlenecks in the current regional energy system’s transition to a low-carbon path. The strong heterogeneity across multiple nodes in the energy system and the inconsistent granularity of data collection make it difficult to accurately allocate carbon-emission responsibilities (Slamersak et al., 2022; Zhang et al., 2023). There are problems of lag and distortion in the transmission of carbon information across supply chain levels, leading to frequent resource mismatches and diminishing marginal benefits of scheduling (Jiang et al., 2024; Zampou et al., 2022). Regional energy demand is highly volatile, and traditional load forecasting methods are difficult to adapt to the rapid pace of data changes and structural complexity, thereby affecting overall configuration accuracy. This phenomenon shows that data heterogeneity and forecast distortion jointly increase the risk of a structural increase in marginal emission-reduction costs. Under the carbon quota control mechanism, supply chain companies lack effective technical means to make cost-oriented emission-reduction decisions, leading to high marginal emission-reduction costs for a long time (Onukwulu et al., 2021; Xu et al., 2023).

To alleviate the above problems, existing research has proposed a series of solutions from the perspectives of optimisation models, prediction algorithms, and information platform design. In terms of optimisation modelling, most studies use linear or nonlinear programming models to construct a regional energy configuration framework, but most of them do not introduce marginal measurement indicators of emission costs and lack a complete evaluation of system benefits under carbon constraints (Mao et al., 2024; Pallikodathan et al., 2025). At the prediction level, some methods introduce time series models, long short-term memory networks, and other algorithms for load forecasting, which have problems such as insufficient feature dimension selection and a weak response mechanism, and the prediction accuracy has a great impact on subsequent scheduling (Bacanin et al., 2023; Li et al., 2022). In terms of carbon information management, some studies have used blockchain technology to build a carbon ledger. Still, the design of on-chain contract logic and the efficiency of system deployment remain immature. While these methods improve the performance of some links, they have not formed a complete integrated coordination mechanism of scheduling, forecasting, and verification, and it is still difficult to effectively reduce the marginal emission reduction cost of regional energy systems under carbon constraints (Lameh et al., 2022; Wu et al., 2023).

To address the high marginal cost of reducing emissions in regional energy systems under carbon quota constraints, this paper constructs a digital scheduling framework that integrates MILP with a carbon information trust mechanism. This paper constructs a resource allocation network covering multiple energy types, such as electricity and heat, using an MILP model, embeds carbon quota restrictions and energy conversion efficiency coefficients into the model objectives and constraints, and incorporates node-level supply and demand constraints into the model objectives and constraints, thereby enabling low-carbon optimisation control of the scheduling scheme. This paper uses XGBoost to construct a daily-scale load forecasting module for regional energy consumption. The input features include meteorological variables, electricity price series, and characteristics of industrial energy consumption. The output prediction results drive real-time MILP parameter updates to achieve a dynamic closed loop for the model input. This paper designs a lightweight Hyperledger Fabric chain code to implement emission data chaining, node responsibility quantification, and a carbon information synchronisation mechanism, ensuring the traceability and verifiability of each node's marginal emission reduction effect. The chain code mechanism is deeply integrated with the MILP scheduling model, so that the carbon emission data generated by each round of optimised scheduling can be stored and verified on the blockchain in real time, enabling a two-way closed loop between scheduling and verification. The system provides instant feedback on optimisation plans via the on-chain responsibility matrix and over-emission alarm logic, improving the accuracy of carbon-constraint responses and governance transparency.

2 Related work

Against the backdrop of carbon constraints, the optimisation scheduling strategy for regional energy systems continues to evolve towards a coordinated approach of low-carbon and economic development. Li et al. (2023) optimised the allocation of carbon emission quotas and constructed a carbon trading model through the entropy weight method. Combined with the additional carbon-emission impact of wind power access, they established a day-ahead optimal scheduling model to minimise total system cost, effectively balancing economic and low-carbon objectives, and verified the feasibility of the strategy through simulation. The core idea is to enhance the energy system's low-carbon dispatch flexibility during dynamic load regulation by introducing multiple carbon cost constraints (Sun et al., 2024; Zhang et al., 2024). To further improve the energy system's ability to respond to market signals, Tang et al. (2023) developed a regional integrated energy system optimisation model that accounts for carbon-trading costs and dynamic demand response. They used the improved Nondominated Sorting Genetic Algorithm II (NSGA-II) algorithm to verify it. They found that optimising demand response can improve energy efficiency and achieve coordinated optimisation of economic and low-carbon goals. To enhance the model's coordinated response to the uncertainty of renewable energy and the diversity of carbon-emission-reduction measures, a multi-level low-carbon technology integration mechanism was further introduced (Zhang et al., 2024). Sun et al. (2024) integrated renewable energy forecasts through K-means clustering, combined carbon capture and demand-side response to build a comprehensive energy model, and achieved low-carbon resource optimisation allocation and economic scheduling goals through multi-scenario verification. Most of the above studies focused on the optimisation of a single node or a single energy type. They failed to fully reflect the carbon-emission coupling mechanism of the regional energy system, given its structural characteristics of multi-energy complementarity, cooling, heating, and electricity coordination, as well as cross-node resource allocation. On the one hand, the energy flow and carbon flow in the multi-energy system are highly coupled in time and space dimensions, and the marginal emission reduction effects are difficult to superimpose linearly; on the other hand, the coordinated coordination of power distribution, heating, and gas sources between nodes constitutes a dynamic constraint on the marginal carbon cost. Most existing models have not incorporated it into a unified scheduling framework, making it difficult to achieve system-level marginal optimisation analysis.

In the context of the digital economy, the integrated application of energy supply chain and carbon-emission data governance is accelerating, and various studies are exploring technology-driven approaches to improve system operational efficiency and emission management capabilities. Fu et al. (2023) constructed enterprise-level indicators based on three-stage data envelopment analysis (DEA) and content analysis, and found, using a two-way fixed-effect model, that the digital economy significantly improves the efficiency of the energy supply chain through regional industrial agglomeration and enterprise technological innovation. The effect is more prominent in large enterprises, non-state-owned enterprises, and highly market-oriented regions. This research logic outlines the mechanisms of the two-way penetration of digital technology at the macro-governance and micro-enterprise levels, which help promote cross-level collaboration to enhance supply chain resilience and low-carbon transformation capabilities (Wang and Zhao, 2023; Yang et al., 2024). To further promote transparent governance of transnational energy supply chains, Heeß et al. (2024) taking the international hydrogen supply chain as an example, proposed that digital product passports must have core design principles such as comprehensive automatic data collection, decentralised tamper-proof processing, privacy protection, and interoperability to solve the problem of sustainability verification of global supply chains. This idea further extends the application boundaries of digital governance tools in the trusted flow of cross-organisational data and the integrity of carbon information. It provides structural support for emission supervision under multi-agent collaboration (Zhang and Seuring, 2024). Stroher et al. (2025) proposed a technical solution that breaks through organisational boundaries by building an automated supply chain carbon data sharing framework that integrates digital technologies to systematically improve carbon accounting accuracy and fill the accounting gap in supply chain scope 3 emissions, thereby promoting the digital collaborative development of a sustainable supply chain ecosystem. Although these studies demonstrate the multidimensional possibilities of digital governance in terms of methods and tools, they still face problems such as a lack of uniformity and difficulties in practice regarding regional adaptability, data collaboration standards, and actual implementation paths. Especially at the core technology level of the digital economy, smart contracts, as programmable governance units, offer the technical advantages of embedded rules, automatic execution, and real-time accountability. They can embed marginal-constraint logic into the mapping of carbon emission rights and responsibilities, integrate with scheduling optimisation results, and establish a closed-loop feedback path between scheduling plans and carbon data verification. However, most existing research remains at the stage of on-chain ledger construction. It has not yet deeply integrated the smart contract mechanism with the objective function or constraint structure of the scheduling optimisation model, nor has it addressed the design of collaborative mechanisms in the marginal-emission-reduction-cost-optimisation scenario.

3 Construction of digital dispatch mechanism driven by low carbon

3.1 Multi-node energy-carbon collaborative optimisation model based on MILP

Under the dual drivers of carbon constraints and multi-energy collaboration, the regional energy system's supply chain needs to achieve dynamic resource matching and link carbon emission accounting from source energy collection to terminal consumption.

To achieve this goal, a MILP model is constructed. By introducing a resource allocation matrix and a carbon responsibility mapping mechanism, the power generation, transmission, distribution, and terminal energy consumption nodes are coordinated in a unified scheduling framework to achieve full-chain optimisation under the minimum unit marginal emission reduction cost (Laing et al., 2022; Sheikh et al., 2025).

The first step before building a multi-node energy-carbon synergistic optimisation model is to specify the system's initial state to clarify the benchmark for calculating marginal emission-reduction costs. The first state is the common price of the energy system, as well as the carbon emissions of the regional energy system under current operating conditions without optimised scheduling. Initial costs are determined from the actual operating costs of different nodes across historical scheduling cycles, including power generation, transmission, and distribution, and end-use energy. They are aggregated using a single statistical criterion. Primary emission scales are determined from measured energy consumption and the corresponding emission rates of individual nodes at the same point in the energy flow chain. They are summed along the length of the energy flow chain. The previous data are derived from historical records of regional scheduling and energy statistics, and they are consistent with the optimisation model due to the time scale and node division criteria. This state is compared to the cost and emission outcomes generated in the optimisation stage. The total difference quantifies the change in cost attributable to the unit reduction in emissions before and after, thereby establishing that the marginal cost of emission reduction has a single, calculable basis.

To account for the nonlinear behaviour of energy conversion efficiency in high-emission devices (such as gas turbines and large-scale industrial boilers), a piecewise linear approximation (PLA) method is employed. The nonlinear efficiency curve $f(x)$ of these devices is partitioned into K segments based on their operating range. For each segment $k \in \{1,\ldots,K\}$, we introduce auxiliary continuous variables Δx_k and binary variables z_k:

$$x = \sum_{k=1}^{K} \Delta x_k, \quad f(x) \approx \sum_{k=1}^{K} (s_k \cdot \Delta x_k + z_k \cdot b_k) \tag{1}$$

where s_k represents the slope of the k th segment, and b_k is the intercept. To ensure the sequential activation of segments, the SOS2 (Special Ordered Sets of type 2) constraint is applied, requiring that at most two adjacent variables can be non-zero. This structure transforms the original non-convex efficiency optimisation problem into a set of linear constraints, enabling the MILP solver to efficiently find the global optimum for carbon emission intensity and resource allocation.

The model objective function is defined as minimising the unit benefit from emission reduction. The cost function is constructed by comparing the total carbon emissions of the system before and after scheduling with the cost input level, as shown in formula (2):

$$minC_{mec} = {C_t - C_t^0} \Big/ {E_c^0 - E_c} \tag{2}$$

In formula (2), C_{mec} represents the unit marginal emission-reduction cost, C_t and C_t^0 represent the total system costs after scheduling optimisation and in the initial state, respectively, and E_c^0 and E_c represent the total carbon emissions in the initial and optimised states, respectively. Through the constraint-nesting construction of the objective function, the coupled mapping between resource flows and node behaviour under carbon quota control is realised.

To achieve synchronous control of the energy and carbon responsibility flows across the whole system, the node-level energy balance relationship is introduced in the model constraint layer, stipulating that the input and output power of each node at each moment must satisfy the conservation principle. The specific expression is shown in formula (3):

$$d_j = \sum_{i \in I} x_{ij} \cdot \eta_{ij} - \sum_{k \in K} x_{jk} \; \forall j \in J \tag{3}$$

In formula (3), x_{ij} represents the amount of resource transmission from node i to node j, η_{ij} represents the corresponding energy conversion efficiency, 3 x_{jk} represents the resource flow output from node j to the downstream node k, and d_j represents the load demand of node j. The energy balance constraint ensures that the scheduling model maintains a closed loop of energy flow during transmission and conversion.

To address carbon emission constraints, the node-level carbon factor and quota cap are introduced to ensure each node's emissions do not exceed the permitted level via a linear expression. The constraint form is shown in formula (4):

$$\sum_{i \in I} x_{ij} \cdot \alpha_{ij} \le \theta_j \; \forall j \in J \tag{4}$$

In formula (4), α_{ij} represents the carbon emission factor during the transmission of unit energy from i to j, and θ_j represents the upper limit of carbon emissions of node j in this scheduling cycle. The introduction of carbon constraints effectively limits the weight of high-emission paths in resource allocation and ensures that system operation complies with the regional carbon peak policy orientation.

The model variables include two types of decision variables: continuous and discrete.

1 *Continuous variables*: The primary continuous variable is $x_{ij,t}$, representing the resource flow amount from node i to node j at time t. These variables directly participate in the objective function (equation (2)) by determining the total cost C_t and total emissions E_c. They are also constrained by the energy balance (equation (3)) and carbon emission limits (equation (4)).

2 *Discrete variables*: To manage device operations and path selection, two sets of binary variables are introduced: $u_{m,t} \in \{0,1\}$ denotes the startup/shutdown status of device m at time t, where $u_{m,t} = 1$ indicates the device is operational. This variable is used to enforce minimum-power constraints and startup costs; $C_t.v_{ij,t} \in \{0,1\}$ indicates whether the transmission path between nodes i and j is active.

These discrete variables provide the logical basis for the MILP model to dynamically select optimal energy paths and equipment schedules, ensuring that the system minimises the unit marginal emission reduction cost C_{mec} while maintaining operational feasibility.

To strengthen the consistency between the visual framework and the mathematical formulation, the 'energy-logistics joint scheduling structure' depicted in Figure 1 is directly mapped to the MILP constraints. Specifically:

Energy balance mapping (equation (3)): Each node in Figure 1 (represented as supply, conversion, or demand points) corresponds to the conservation law in equation (3). The arrows representing resource flows $x_{ij,t}$ ensure that the sum of energy inputs and local generation at any node in the diagram equals the sum of outputs and local consumption.

Carbon emission mapping (equation (4)): The 'Carbon Monitoring Layer' in Figure 1 provides the real-time carbon intensity coefficients used in equation (4). This ensures that the cumulative emissions from all logistics paths and energy conversion nodes identified in the diagram do not exceed the dynamic carbon quota L_{quota} imposed by the constraint. This mapping ensures that the logistics-driven scheduling logic in the diagram is strictly constrained by the MILP model's physical and environmental limits.

Figure 1 Regional energy-logistics joint scheduling structure (see online version for colours)

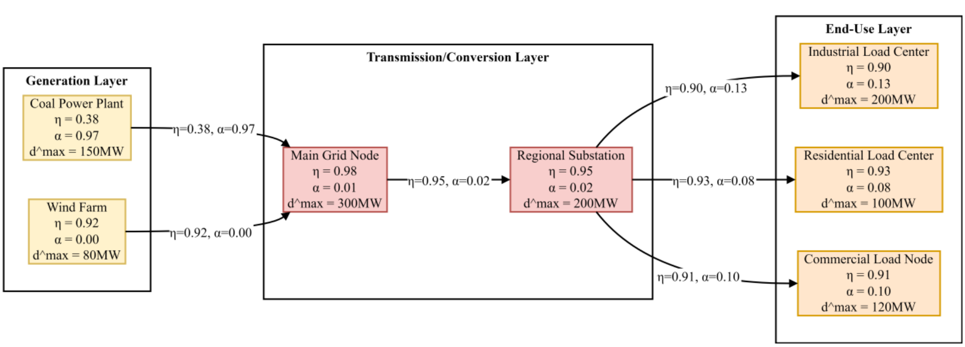

The model input parameters include node type, energy type, conversion efficiency matrix, carbon emission factor, and load boundary, and their main values are shown in Table 1. Table 1 distinguishes parameter categories by node level and clarifies the linear correspondence between various resource types and emission factors, providing multidimensional basic data support for the scheduling model.

Table 1 Regional energy system node configuration parameters

Node type	*Node name*	*Energy type*	*Conversion efficiency*	*Carbon emission factor*	*Maximum load (MW)*
Generation	Coal-fired Unit	Coal	0.38	0.97	150
Generation	Wind Farm	Wind	0.92	0.00	80
Transmission	Main Grid Node	Electricity	0.98	0.01	300
Transmission	Regional Substation	Electricity	0.95	0.02	200
Consumption	Industrial Load Centre	Industrial	0.90	0.13	200
Consumption	Residential Load Centre	Residential	0.93	0.08	100
Consumption	Commercial Load Node	Commercial	0.91	0.10	120

3.2 *Load forecasting and scheduling linkage based on XGBoost*

To improve the dynamic adaptability of the regional energy system scheduling model, this section constructs a linkage mechanism that integrates load forecasting and resource allocation, and introduces XGBoost to predict the daily load of the multi-node regional energy system to achieve real-time update of the boundary conditions of the optimisation model (Luo et al., 2024; Wang et al., 2026).

To ensure the predictive accuracy and generalisability of the XGBoost model, the key hyperparameters were meticulously tuned. Specifically, the learning rate (eta) was set to 0.05 to prevent overfitting, the maximum tree depth (max_depth) was set to 6 to capture complex nonlinearities in load fluctuations, and the subsampling ratio (subsample) was maintained at 0.8. These hyperparameters were optimised via a 5-fold cross-validation grid search on the training set. The search space for the grid search included learning rates from 0.01 to 0.1 and max_depth from 3 to 10. This systematic approach ensures the reproducibility of the load and emission boundary predictions, providing a stable input for the subsequent MILP scheduling model.

In the input feature design, four types of information are included: node historical load series, electricity price signals, industrial activity intensity, and meteorological variables. The training set covers the change samples in typical daily, weekly, and seasonal cycles. The load forecast target is based on the node-level hourly load. The load sequence function is trained using supervised learning to produce a rolling forecast for the next 24 h.

The integration between the XGBoost prediction module and the MILP scheduling model is implemented through a specialised data exchange layer.

1 *Bidirectional interface*: The prediction model outputs the forecasted load and carbon intensity data to the MILP model in JSON format. In contrast, the MILP model feeds back the actual device operation status and resource allocation results to the XGBoost module. This feedback serves as 'online learning' data to refine feature engineering in the next cycle.

2 *Asynchronous mechanism*: To resolve the time-scale mismatch between the high-frequency prediction (15-minute intervals) and the global optimisation (1-h intervals), an Asynchronous Message Queue (based on RabbitMQ) is employed. The prediction module pushes data to the queue independently, and the scheduling model pulls the latest 'time-stamped' boundary conditions at each trigger point.

3 *Time consistency*: A global synchronous clock (GSC) and a 'Sliding Window Buffer' are used to ensure that the data being optimised corresponds to the correct physical time segment, preventing any latency-induced decision errors.

Assuming that the input feature vector is $\mathbf{x}_{i,t} = [p_{i,t}^{elec}, w_t, h_{i,t}, a_t]$, $p_{i,t}^{elec}$ is the historical electricity price of node i at time t, w_t is the combination of meteorological variables at time t, $h_{i,t}$ is the historical load sequence, and a_t is the industrial activity intensity factor. The load forecasting function is modelled as:

$$\hat{L}_{i,t+1} = f_{XGB}(\mathbf{x}_{i,t}) \tag{5}$$

In formula (5), $\hat{L}_{i,t+1}$ is the load value of the predicted node i at time $t+1$, and f_{XGB} is the trained XGBoost model.

The prediction results are transmitted to the MILP model in real time as input parameters to correct the load constraints and carbon-emission boundaries for each node. By building a two-way interface, the scheduling model obtains the latest prediction data after each round of operation, and the actual scheduling is fed back to iteratively update the prediction model, forming a closed-loop system. In the software architecture, this mechanism relies on an asynchronous interface between the scheduling control layer and the prediction calculation layer, balancing scheduling frequency and prediction accuracy while ensuring efficient matching of multi-node resources in the timing dimension.

The preprocessing procedures and time range were uniformly defined, and the partitioning ratio was defined before training the load forecasting model. The data chosen were the hourly continuous operation records of the regional energy system for 2021–2023, covering the full year cycle. The training and test sets were split into a chronological sequence: the initial 80% of the training set was used to train the model, and the remaining 20% was used as an independent test set to ensure temporal stability and objectivity in the evaluation results.

The preprocessing step replaced missing data with interpolated values and removed abnormal fluctuations to ensure sequence stability. For the various dimensional traits, a min-max normalisation technique was employed to map the historical load, electricity prices, meteorological variables, and the intensity of industrial activity to the same range of values, thereby minimising the interference of scale variation on the model's weight distribution. The optimised model was then trained on the parameter-optimised data and cross-validation results to create a stable forecast structure and provide a stable basis for boundary scheduling optimisation.

The input feature combination and accuracy evaluation results for the prediction module are shown in Table 2, which presents the mean absolute error (MAE) and root mean square error (RMSE) for different variable combinations. The prediction accuracy is optimal when combining four-dimensional input features, with MAE stable within 8.1 MW and RMSE not exceeding 11.4 MW.

Table 2 Comparison of prediction model input features and accuracy evaluation

Feature set ID	*Input variable dimension*	*MAE* (MW)	*RMSE* (MW)
A	Historical Load Sequence	13.5	17.8
B	Historical Load + Electricity Price	10.9	14.3
C	Historical Load + Electricity Price + Weather Variables	9.3	12.2
D	Historical Load + Electricity Price + Weather + Activity Intensity	8.1	11.4

The overall structure of the linkage mechanism is shown in Figure 2, which illustrates the data channel connection method and the parameter update path between the prediction module and the scheduling model, reflecting two-way feedback and parallel update capabilities. The prediction results are transmitted to the MILP module via the preprocessing interface, and the scheduling output feeds back into the feature weight correction logic to ensure that the prediction deviation converges within the error tolerance threshold round by round, thereby improving the overall scheduling response capability of the system.

Figure 2 Bidirectional linkage mechanism of forecasting and scheduling (see online version for colours)

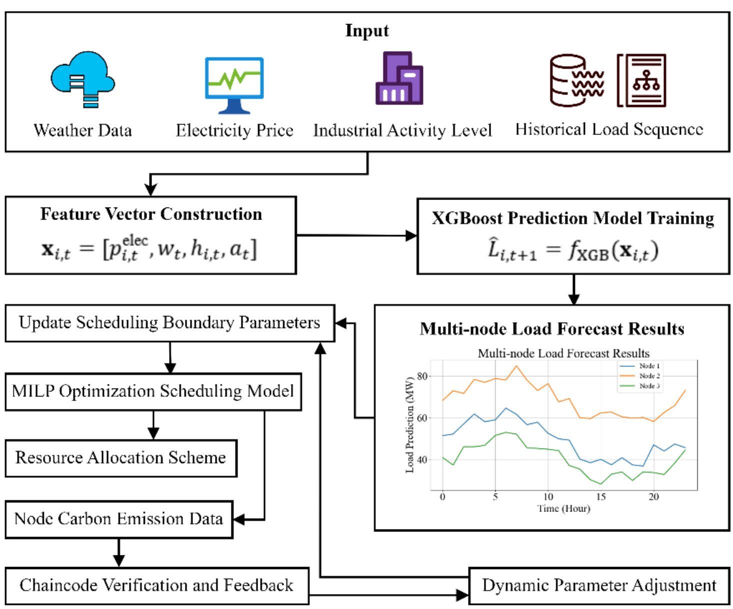

This linkage mechanism maintains real-time scheduling while strengthening the system's robustness under multi-source heterogeneous inputs, providing a technical basis for the regional energy system to achieve low-cost, high-efficiency operation under carbon constraints. Improved prediction accuracy directly reduces the proportion of resource mismatch and redundant configuration, optimises the boundary structure of scheduling parameters, and enhances the system's ability to respond to uncertain disturbances.

3.3 Carbon data verification and mapping based on hyperledger fabric chain code

In constructing the carbon information chaincode mechanism based on Hyperledger Fabric, the system adopts a lightweight channel structure to match the operational characteristics of multi-node collaboration and high-frequency emission accounting in regional energy systems. The chaincode needs to form a nested deployment relationship with the scheduling model. If a single global channel is used, all nodes participate in the endorsement and sorting of emission data, thereby expanding the scope of consensus and prolonging block confirmation time, weakening the efficiency of real-time on-chain scheduling. To maintain the time consistency between on-chain verification and optimisation computation, the system divides channels according to the business relationships of nodes, restricting the flow of emission data related to power generation, transmission, and distribution, and terminals within the corresponding participating entities, thus compressing the transaction propagation path and verification scale at the structural level.

In this architecture, the scheduling model's node emission output is directly hashed, with responsibilities assigned and consistent across channels. Irrelevant nodes are not subject to the verification process, reducing redundant broadcasting and repeated computation and improving chaincode execution performance and data write throughput. The system ensures overall consistency of the ledger state across channels by synchronising key digest information via anchor nodes, establishing a tightly coupled, closed-loop system between carbon data notarisation, responsibility quantification, and scheduling optimisation. This guarantees that the on-chain governance mechanism and the various scheduling cycles are synchronised in the operation rhythm.

To achieve a 'bidirectional closed loop' between the governance and optimisation layers, the Hyperledger Fabric chaincode is deeply integrated with the MILP model via an automated data-triggering mechanism. The execution sequence is as follows:

Forward verification: Before the MILP model executes, the chaincode retrieves the historical carbon quota and emission balances from the ledger as initial boundary conditions. Only data verified by the consensus nodes can be used as valid inputs for the constraint L_{quota} in equation (4).

Real-time feedback: Once the MILP solver generates the optimal scheduling result (including resource flow $x_{ij,t}$ and startup status $u_{m,t}$), the 'Event Listener' within the chaincode automatically captures these decisions.

State update and arbitration: The chaincode calculates the projected emissions based on the scheduling plan. If the result deviates from the physical sensor data by more than the threshold, the 'Error Arbitration Function' is triggered to adjust the model's weight parameters for the next period. This architecture ensures that the MILP model is not an isolated calculator but is constrained by and feeds back to a tamper-proof 'Truth Source' on the blockchain.

The logic core of the chain code revolves around the node emission data output by the scheduling model for regular chain processing. Assuming that the emission of the i th node in the regional energy system in time period t is E_i^t. This data is output by the MILP model and is defined as follows:

$$E_i^t = \sum_{j \in S} \alpha_{ij} \cdot x_{ij}^t \tag{6}$$

In formula (6), x_{ij}^t represents the energy flow on the energy transmission path in time period t. Each item $\alpha_{ij} \cdot x_{ij}^t$ represents the emission measurement under a single path.

In the chain code deployment logic, the on-chain state variable E_i^t stores the emission data calculated by the scheduling model, which is encrypted using a Merkle tree to ensure tamper resistance. The hash function is set to $h(\cdot)$, and the storage value is defined as:

$$E_i^t = h(E_i^t \,\|\, t \,\|\, ID_i) \tag{7}$$

In formula (7), $\|$ represents the connection operation, ID_i is the unique identifier of node i, and $h(\cdot)$ ensures the encryption consistency of data throughout its entire life cycle on the chain.

The responsibility mapping mechanism automatically generates the responsibility matrix $R \in R^{n \times T}$ through the chaincode contract. The matrix element R_{it} represents the proportion of node i 's responsibility for the total emissions of the system in time period t, which is defined as follows:

$$R_{it} = E_i^t \Big/ \sum_{k=1}^{n} E_k^t \tag{8}$$

Threshold judgement logic is embedded in the chain code deployment process. When the carbon emissions of any node in any period exceed its carbon quota $\overline{E}_i^t$, the contract alarm mechanism is triggered. The formula is as follows:

$$\delta_i^t = \begin{cases} 1, & \text{if } E_i^t > \overline{E}_i^t \\ 0, & \text{otherwise} \end{cases} \tag{9}$$

In formula (9), δ_i^t is the over-emission identification variable. When the value is 1, the chain code will push an alarm message to the supervisory node and freeze the energy allocation right of the node in the next period until a new carbon responsibility agreement is reached. The chain code design also includes a mechanism for verifying cross-node carbon data consistency. Supposing there are two adjacent nodes i and j, the transmission emissions recorded on their chains should satisfy the symmetric relationship:

$$| E_{ij}^t - E_{ji}^t | \le \epsilon \tag{10}$$

In formula (10), E_{ij}^{t} represents the transmission emission recorded by node *i* to node *j*, E_{ji}^{t} represents the acceptance emission recorded by node *j*, and ϵ is the upper limit of the consistency tolerance set by the system. If this condition is not met, the chain code will automatically trigger the error arbitration function, recalculate the scheduling allocation on the path, and call the smart contract to restart the on-chain data mapping and update process.

To ensure the integrity and non-repudiation of carbon emission data, the smart contract (chaincode) implements a Consistency Verification Mechanism and an Error Arbitration Function. The specific logic flow is as follows:

1 *Consistency verification mechanism*: When a node submits carbon data D_i, the chaincode automatically triggers a verification script. It compares D_i with the historical emission trend H_i and the energy balance constraints B_j stored on the ledger. If $|D_i - f(H_i, B_j)| > \epsilon$ (where ϵ is the pre-defined tolerance threshold), the data is flagged as 'Pending' rather than being committed to the global state.

2 *Error arbitration function*: For flagged data, the arbitration function is invoked. It adopts a multi-signature consensus approach in which N representative nodes (e.g., regulatory agencies and grid operators) recalculate based on raw IoT sensor logs. The pseudo-code for the arbitration logic is defined as: Function ErrorArbitration(Data_ID, Votes):

```
Threshold = (2/3) * Total_Auditors
If Valid_Votes(Votes) > Threshold:
    UpdateState(Data_ID, 'Verified')
Else:
    RejectData(Data_ID, 'Audit_Failure')
```

This dual-layer mechanism ensures that the marginal emission-reduction cost calculated by the MILP model is based on authentic, verified terminal data.

4 Experimental platform and test setup

4.1 Experimental system construction and platform deployment

The numerical data in this paper are based on historical dispatch records and the energy statistical yearbook of the Suzhou regional energy system in Jiangsu Province, China. The historical dispatch data cover power generation, transmission, and distribution, as well as end-user energy nodes in Suzhou Industrial Park, for the period from 2021 to 2023, with hourly granularity. It captures node outputs, the scale of energy transmission, and the respective emission accounting results to aid in dispatch and load forecasting modelling. To validate the overall energy consumption, structural proportions, and emission factor parameters, the period 2018–2023 is selected from the Suzhou sub-statistics in the Suzhou Provincial Energy Statistical Yearbook, with annual energy statistics as the data granularity. The conversion efficiency and emission factor are determined based on the carbon factor standard of the intergovernmental panel on climate change (IPCC). The samples of fluctuations in the actual load curve for the region mentioned above between 2021 and 2023 are normalised and fed into the model. The Monte Carlo method is used to simulate the system's reaction to disturbances under high levels of uncertainty to assess its properties.

The experimental platform adopts a modular design, integrating three functional modules: scheduling optimisation, load forecasting, and carbon data verification, covering the power generation, transmission, and distribution, and terminal energy consumption links of the regional energy system.

To ensure seamless integration and data interoperability between the XGBoost module, the MILP solver, and the Blockchain ledger, the experimental platform adopts a gRPC-based (Google Remote Procedure Call) unified interface protocol.

Specifically, the communication between the prediction engine and the scheduling core is defined using Protocol Buffers (proto3), which ensures high-performance, low-latency data serialisation. For external data acquisition from IoT sensors and the terminal monitoring system, the platform uses RESTful APIs with OAuth 2.0 authentication to provide secure, standardised access. This hybrid protocol architecture (gRPC for internal high-frequency calls and REST for external data ingestion) ensures real-time responsiveness and structural integrity across the entire regional energy management system.

The platform's operating environment uses a mainstream high-performance configuration to meet the computing power and data throughput requirements of large-scale scheduling and high-frequency prediction tasks. The specific software and hardware configurations are shown in Table 3.

Table 3 Experimental platform hardware and software configuration

Configuration item	*Model*	*Quantity*	*Function*
CPU	Intel Xeon Gold 6338	2	Scheduling computation and prediction tasks
GPU	NVIDIA RTX 4090 24GB	2	Supports efficient XGBoost training and inference
Memory	DDR4 3200MHz 512GB	1	Large-scale parameter storage and access
Storage Drive	NVMe SSD 4TB	2	Fast data read/write and caching support
Operating System	Windows 11 Professional	1	Provides a unified graphical operating environment
Python Environment	Python 3.10	–	Supports algorithm development and model execution
Optimisation Engine	Gurobi 10.0	–	Solves the MILP scheduling model
Blockchain framework	Hyperledger Fabric 2.5	–	Carbon data recording and responsibility verification module

After the platform is deployed, the dispatch control centre initiates forecasting and resource allocation requests. The system automatically updates carbon emission records after each dispatch round, forming a closed-loop process of forecasting, optimisation, and verification. This deployment structure provides stable, efficient experimental support for multi-scenario testing and cost analysis of marginal-emission-reduction.

4.2 Model parameter setting and test scenario division

During the parameter-setting process for the experimental model, it is necessary to clarify the parameter-setting method and the numerical bounds for each key parameter in the optimisation objective function and constraint conditions, to ensure that the mixed-integer linear programming (MILP) model has a feasible solution space under the actual constraints during the scheduling solution process. The energy conversion efficiency parameter is set to the measured ratio during the node energy transmission process and is corrected based on the actual regional carbon emission factor data.

While the baseline parameters in Table 1 (e.g., conversion efficiency and carbon factors) are derived from industry standards, we further evaluate the model's robustness by treating them as time-varying rather than fixed constants. Specifically, the conversion efficiency η_m of energy devices is modelled as a function of the ageing degree and ambient temperature. At the same time, the carbon factor γ_j of the power grid is updated hourly based on the real-time energy mix (renewables vs. fossil fuels). To address this uncertainty, a sensitivity analysis was performed by introducing $\pm 15\%$ fluctuations in these key parameters. The results demonstrate that the MILP model, guided by XGBoost's dynamic boundary predictions, maintains a stable marginal cost reduction (within a 3.2% variance range). This confirms that the proposed framework is resilient to the inherent uncertainty and time-varying nature of supply chain energy data.

It is finally determined that the conversion efficiency ranges of the three types of nodes, namely power generation, transmission and distribution, and terminal energy consumption, are 0.35–0.48, 0.92–0.98, and 0.85–0.91, respectively. The carbon emission factor is set to the standard value per energy type in the national energy statistical database. The coal node is set at 0.82 tCO□/MWh, the natural gas node at 0.46 tCO□/MWh, and the clean energy node at 0. The node load cap is set based on the dispatch's historical maximum load, and the cap fluctuates by 5% in response to cyclical changes in regional industrial activity. The carbon quota cap is set based on the monthly dispatch quota and the regional annual carbon emission reduction target, and the quota constraint intensity is adjusted according to the simulation scenario, with the quota intensity change range set to 80% to 120% of the regular quota.

The experiment divided the scheduling scenarios into five typical categories (S1-S5) to observe the model's response performance in terms of marginal emission-reduction cost, resource allocation efficiency, and carbon information consistency. The parameter settings for each dispatching scenario are shown in Table 4. Scenario 1 (S1) sets a high load peak state, and the daily load peak-to-valley ratio is increased to 1.52 to simulate the impact of concentrated energy fluctuations on the stability of the dispatching model; Scenario 2 (S2) sets a severe load fluctuation state, and sets the load standard deviation increase to 35% to test the linkage efficiency of the prediction and dispatching interface; Scenario 3 (S3) adjusts the carbon quota intensity to 85% of the baseline value to test the cost suppression ability under the low-carbon constraint scenario; Scenario 4 (S4) enables the chain code mechanism to verify the carbon information consistency control effect, and the chain code parameters are configured as the standard contract execution logic in the Hyperledger Fabric v2.2 environment; Scenario 5 (S5) artificially introduces data missing and error disturbances, and the deviation range of meteorological and electricity price data in the simulated prediction input is ±10%, which is used to evaluate the fault tolerance of the prediction mechanism to the scheduling boundary parameters. Each scenario is simulated over a 30-day rolling dispatch cycle with hourly steps, completing daily forecasting, allocation, and carbon accounting to capture the overall impact of load and carbon constraint variations.

Table 4 Scheduling scenario simulation parameter settings

Scenario ID	*Load fluctuation rate (Standard Deviation)*	*Peak-to-valley ratio*	*Carbon quota intensity*	*Chaincode enabled*	*Data error disturbance*
S1	12%	1.52	100%	No	None
S2	35%	1.37	100%	No	None
S3	18%	1.44	85%	No	None
S4	15%	1.41	100%	Yes	None
S5	20%	1.46	100%	No	±10%

5 Results analysis

5.1 Analysis of the changing rules of unit marginal emission reduction cost

The experiment constructed three model comparison schemes and designed an experimental process of gradually tightening the carbon emission cap to explore the impact of changes in the intensity of carbon limit constraints on the cost structure of regional multi-energy system scheduling. The basic solution adopts a MILP scheduling model; on this basis, the XGBoost mechanism is introduced to improve load forecasting accuracy, and the chain code technology is further applied to enhance the credibility of carbon data. During the simulation, the carbon quota cap was set to account for 95%, 90%, 85%, 80%, 75%, 70%, 65%, 60%, 55%, and 50% of the system's historical baseline emissions, indicating that the carbon limit conditions are gradually tightening. The system's emission space is constantly shrinking. The unit marginal emission-reduction cost is calculated for each carbon limit ratio, and the response curves for different schemes are compared in Figure 3.

Figure 3 shows that as carbon quotas are gradually compressed, the unit marginal emission reduction cost of the basic MILP model rises rapidly, from 81 yuan/ton under a 95% carbon limit to 278 yuan/ton under a 50% carbon limit, reflecting the model's insufficient flexible scheduling capabilities in a high-pressure emission reduction environment. After introducing the XGBoost prediction mechanism, the unit emission reduction cost under a 50% carbon limit is 259 yuan/ton, 19 yuan/ton lower than the basic model, mainly due to improved resource scheduling efficiency resulting from reduced load forecast errors. When the chain code mechanism is further integrated, the efficiency of carbon emission data verification is improved, the lag in carbon rights settlement is reduced, and the emission-reduction path is more stable. The unit cost under the 50%

carbon limit is 245 yuan/ton, which is significantly lower than other options. In the context of stricter carbon limits, system scheduling accuracy and the credibility of carbon data are important factors in determining the unit's emission-reduction cost.

Figure 3 Trends in unit marginal emission reduction costs (see online version for colours)

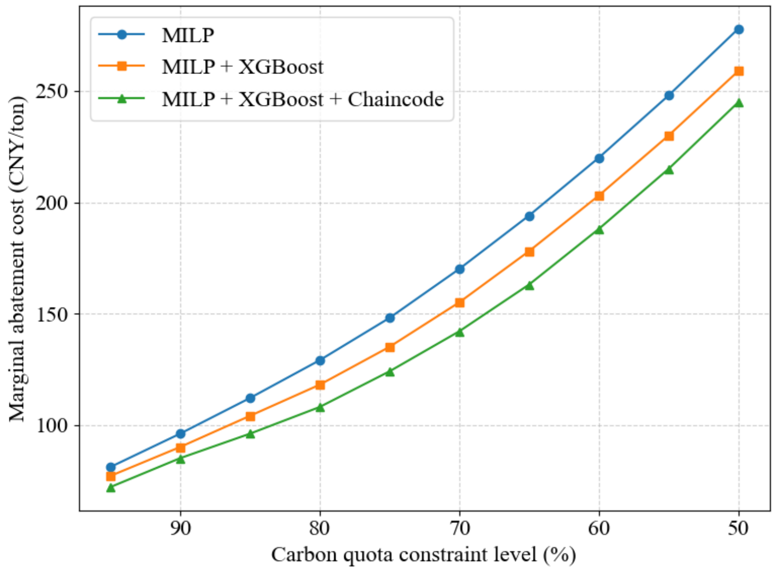

5.2 *Comparison of carbon responsibility allocation structure in multi-node system*

The experiment uses three scheduling models to analyse the structural differences of carbon emission responsibility among nodes in the regional energy system: basic optimisation model (MILP), dynamic optimisation model with load forecasting (MILP + XGBoost), and full-process scheduling model integrating chain code mechanism (MILP + XGBoost + Chaincode), to explore the redistribution characteristics of carbon responsibility in power generation, transmission, distribution, and terminal links under multi-strategy coupling. In the experiment, the power generation nodes are responsible for the initial energy input and the main emission source. The transmission points and distribution nodes serve as intermediate dispatching hubs and are responsible for energy transmission and system stability. The industrial terminals are the downstream energy-consuming nodes with the highest energy intensity and are most sensitive to dispatching plans. The load fluctuations of civil terminals are relatively weak, and they have higher carbon responsibility rigidity. The experiment uses model scheduling to output the carbon-emission proportions of different nodes, thereby describing the distribution of carbon responsibility across each link of the supply chain, as shown in Figure 4.

Figure 4 Multi-node carbon responsibility allocation structure of the regional energy system (see online version for colours)

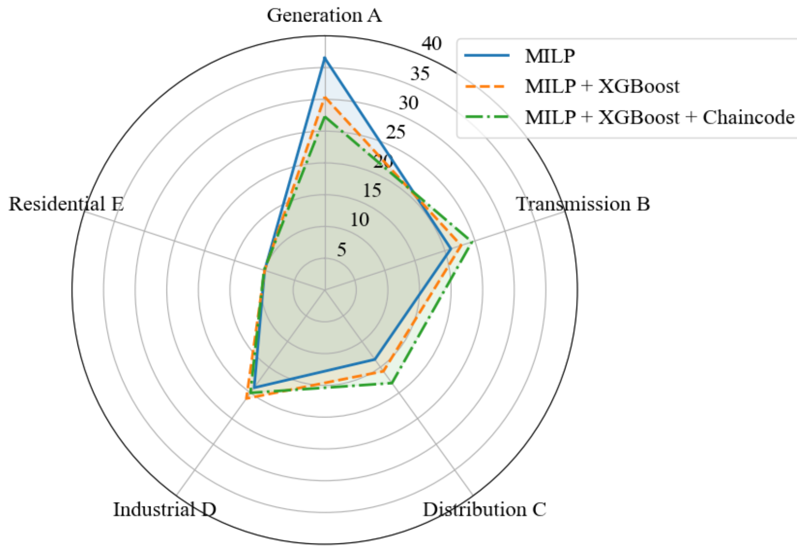

At the power generation node, the carbon responsibility ratio is 36.5% under the MILP model, dropping to 30.4% after the introduction of the load forecasting module. Further, it drops to 27.3% after the introduction of the chain code mechanism. This change is due to the prediction mechanism enhancing the system's ability to respond to changes in terminal energy consumption, thereby allowing part of the emission responsibility to be transferred to downstream nodes along the energy flow path. The introduction of chain code strengthens the traceability of carbon data, aligning emission responsibility sharing more closely with node behaviour characteristics. At transmission nodes, the carbon share increases from 21.0% to 22.7% and then to 24.5%. This is mainly because, after transparency in carbon information is improved, hidden emissions in the energy transmission process are made explicit, thereby increasing the responsibility intensity of the intermediate links. The carbon responsibility of distribution nodes increases from 13.5% to 18.1%, indicating that as the system's sensitivity to network energy efficiency increased, the scheduling model actively shifted part of the emission-reduction pressure to links with large efficiency differences. The carbon responsibility of industrial terminals has changed relatively steadily, always remaining between 19.0% and 21.1%. The reason is that their load elasticity is relatively small, and emission sharing is more restricted by the historical energy consumption structure. The proportion of civil terminals has remained at around 10%, and the responsibility distribution is stable, reflecting that residential energy consumption is subject to strong constraints in system scheduling. Overall, the digital enhancement mechanism of the scheduling model achieves a reasonable redistribution of the carbon responsibility structure without weakening the total carbon consumption constraints.

5.3 *Impact of XGBoost prediction module on system resource allocation efficiency*

To verify the actual impact of the prediction mechanism on the scheduling efficiency of the regional energy system, this paper introduces the XGBoost load prediction module under the five typical scheduling scenarios defined in Section 4.2, and uses the scheduling output without enabling the prediction module as a control, and conducts comparative experiments in three dimensions: resource redundancy rate, energy flow mismatch rate, and spare capacity ratio. The five scenarios involve multiple constraint characteristics, such as peak load, load fluctuation, changes in carbon quota intensity, intervention in the chain code mechanism, and input data disturbance, which can more comprehensively reflect the marginal effect of prediction accuracy on the quality of resource allocation. In the experiment, while keeping other parameters constant, only the prediction module's participation state is adjusted to extract differentiated response characteristics based on the control variables.

To quantitatively evaluate the impact of XGBoost-based predictions on resource allocation efficiency, we introduce the Node Utilisation Coefficient (η_i). It is defined as the ratio of the actual energy throughput to the dynamic capacity limit predicted by the XGBoost model at node i over a scheduling period T. The calculation formula is as follows:

$$\eta_i = \frac{1}{T}\sum_{t=1}^{T}\left(\frac{P_{actual,i,t}}{P_{pred,i,t}\cdot\sigma_{i,t}}\right)\times 100\% \tag{11}$$

where $P_{actual,i,t}$ represents the actual energy flow at node i during time interval t, $P_{pred,i,t}$ is the predicted load requirement from the XGBoost model, and $\sigma_{i,t}$ is the confidence interval coefficient. A higher η_i indicates that the system has achieved a tighter fit between supply and demand through the integration of predictive intelligence and MILP optimisation, thereby reducing redundant energy and lowering marginal costs.

The final result is shown in Figure 5.

Figure 5 Analysis of the impact of XGBoost prediction on system resource allocation efficiency (see online version for colours)

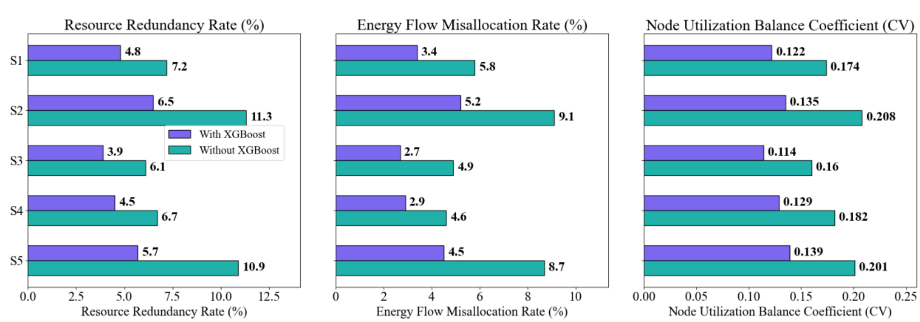

In the S2 scenario, the prediction mechanism compresses the resource redundancy rate from 11.3% to 6.5%. Since the load standard deviation is set to 35% in this scenario, load fluctuations are significantly enhanced. The prediction module mitigates the system's tendency to overestimate the scheduling margin by correcting for extreme node loads in advance. In the S5 scenario, the redundancy rate due to data disturbance reaches 10.9% when XGBoost prediction is not used and drops to 5.7% after prediction is enabled, mainly because the model still maintains strong trend recognition under disturbed input conditions. In terms of energy flow mismatch rate, the two high disturbance scenarios, S2 and S5, drop from 9.1% and 8.7% to 5.2% and 4.5%, respectively. This is because the prediction mechanism adjusts the distribution of energy flow paths to fit the future load structure, thereby reducing the frequency of cross-node mismatches. In terms of node utilisation balance, the prediction mechanism reduces the node utilisation coefficient of variation in the S2 scenario from 0.208 to 0.135, and in the S5 scenario from 0.201 to 0.139. Since the system is prone to local node load aggregation under high volatility or high error input conditions, the prediction mechanism improves the spatial dispersion of task scheduling. The above results show that the XGBoost module effectively improves the compactness, accuracy, and balance of system resource configuration in different scheduling scenarios.

5.4 The role of the chain code mechanism in carbon emission data consistency

To verify the role of the chain code mechanism in the governance of carbon emission information data, this experiment sets up seven consecutive scheduling cycles to record the distribution of carbon emission data consistency indicators (Pearson correlation coefficient and consistency ratio are used here) of the system when the chain code mechanism is enabled and not enabled. It uses box plots to quantify the changes in data discreteness and stability under different states. The data source covers the emission verification results and real-time scheduling feedback of each node in the system, comprehensively reflecting the stability and transparency of the carbon information transmission and mapping process. The results are shown in Figure 6.

Figure 6 Comparison of the impact of the chain code mechanism on the consistency of carbon emission data (see online version for colours)

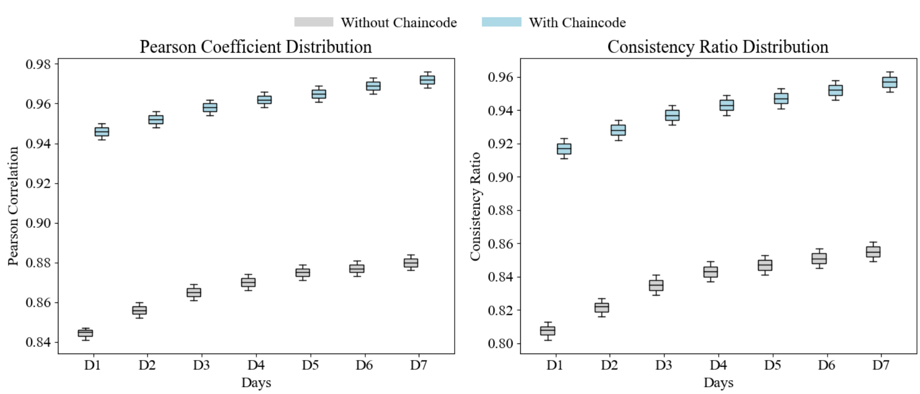

Combined with the results in Figure 6, when the chain code mechanism is not deployed, the minimum Pearson correlation coefficient is 0.841, and the maximum is only 0.884. Due to the lack of effective data encryption and verification methods, there is a risk of data loss and tampering during information transmission between nodes, leading to significant fluctuations in overall correlation. In contrast, after the chain code mechanism is enabled, the minimum Pearson coefficient increases to 0.942, and the maximum stabilises at 0.976, reflecting the structural strengthening effect of the chain code contract on data synchronisation and traceability, and significantly improving the full-chain consistency of emission data. In the consistency ratio indicator, when the chain code is not deployed, the minimum value is 0.802, and the maximum is 0.861, indicating that the system's carbon data mapping accuracy is limited. This is mainly due to the vague division of node responsibilities under the traditional information management model, and the data mapping link is susceptible to interference. After the chain code mechanism intervened, the consistency ratio increases overall, with the minimum value reaching 0.911 and the maximum value stabilising at 0.963, indicating that the chain code structure effectively constrains the carbon information transmission chain, and the overall consistency and transparency of the system data are improved, verifying the positive role of the chain code mechanism in promoting the governance of carbon emission information.

5.5 Analysis of system response characteristics under different carbon limit intensities

Under different carbon intensity limits, the response law within the regional energy system directly affects the overall cost and stability of the low-carbon transformation. To deeply reveal the system's coordination ability, supply-and-demand balance, and resource-allocation efficiency under the background of tightening carbon constraints, this section sets the carbon intensity range from 95% to 50%.

To better quantify the system's ability to handle load volatility and tightening carbon quotas, we define the Scheduling Flexibility (F_{flex}) metric. This metric represents the feasible adjustment range of the system's energy output relative to its total capacity while satisfying all carbon constraints. The formula is defined as:

$$F_{flex} = \frac{\sum_{t=1}^{T} (P_{max,t}^{carbon} - P_{min,t}^{carbon})}{\sum_{t=1}^{T} P_{cap,t}} \times 100\% \tag{12}$$

where $P_{max,t}^{carbon}$ and $P_{min,t}^{carbon}$ are the maximum and minimum feasible power outputs at time t under the current carbon quota and MILP constraints, and $P_{cap,t}$ is the total installed capacity. A higher F_{flex} indicates that the integrated XGBoost-MILP framework provides greater 'manoeuvring space' for the supply chain to reconfigure resources without violating emission limits, even under 50% carbon quota compression.

By constructing a joint scheduling model, the changing trends of three core indicators, namely system scheduling elasticity, load suppression level, and energy flow mismatch rate, are measured in turn, reflecting the multidimensional impact of the gradual tightening of carbon limits on the system operation characteristics. The experimental results are shown in Figure 7.

Figure 7 Changes in system multidimensional response under different carbon limit intensities (see online version for colours)

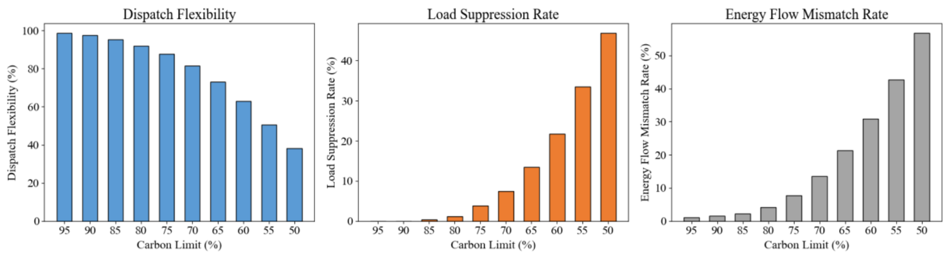

When the carbon intensity limit is maintained at 95–80%, the system scheduling elasticity is always above 92%. At this stage, there is a sufficient resource surplus within the energy supply chain, the node coordination configuration is not seriously disturbed, and the system has strong dynamic adjustment capabilities. As the carbon intensity limit drops to 75%, the scheduling flexibility drops to 87.6%, mainly because some high-carbon-emitting nodes are restricted, leading to controlled resource output and a decrease in the system's overall flexibility. Further tightening the carbon limit to 60%, the scheduling flexibility drops to 62.8%, and the load suppression rate climbs to 21.7%. The reason is that the load supply capacity of low-efficiency nodes has weakened, and conventional scheduling methods cannot fully offset the gap caused by the restrictions imposed by high-carbon nodes, so part of the system's energy demand is forced to be reduced. When the carbon limit intensity is reduced to 50%, the load suppression rate rises to 46.9%, and the energy flow mismatch rate rises to 56.8%. This indicates that there is a serious misalignment of resources within the system, the coordinated efficiency of carbon emissions and energy flows between nodes is greatly reduced, and the structural contradictions in the scheduling process are prominent. The overall results show that when the carbon intensity is below 70%, the system's coordination, supply-and-demand balance, and resource allocation capabilities are significantly weakened. Excessively strict carbon constraints will directly increase operational risks in the energy supply chain.

5.6 Analysis of convergence efficiency of carbon emission reduction paths

To measure the effects of various scheduling mechanisms on the dynamic behaviour of carbon-emission-reduction trajectories in regional energy systems, this paper conducts multi-round continuous simulations under the same carbon quota constraint. The integrated prediction model, the model with an additional integrated chaincode mechanism, and the MILP model are compared to identify fluctuations in cumulative carbon emissions as the scheduling cycle approaches the completion of the process. The time period t in this analysis model is the hourly time step at which the resource flow is calculated, and the model's emissions are counted, to show the current state of energy flow and node emissions over one day. The scheduling cycle is the outer time unit of the system for executing one complete functioning cycle, which includes the entire process of load forecasting, optimal allocation, carbon verification, and feedback of the results, with a scale set at the daily level. The daily cycle of scheduling spans an hour; the former is taken to represent the sum of daily emissions, whereas the latter describes the development pattern of the cumulative emission trajectory over the days. The convergence rate, variation properties, and control of cumulative emission curves under various mechanisms are compared using rolling simulations in continuous multi-day scheduling cycles in Figure 8.

Figure 8 Convergence comparison of carbon emission reduction paths under different scheduling mechanisms (see online version for colours)

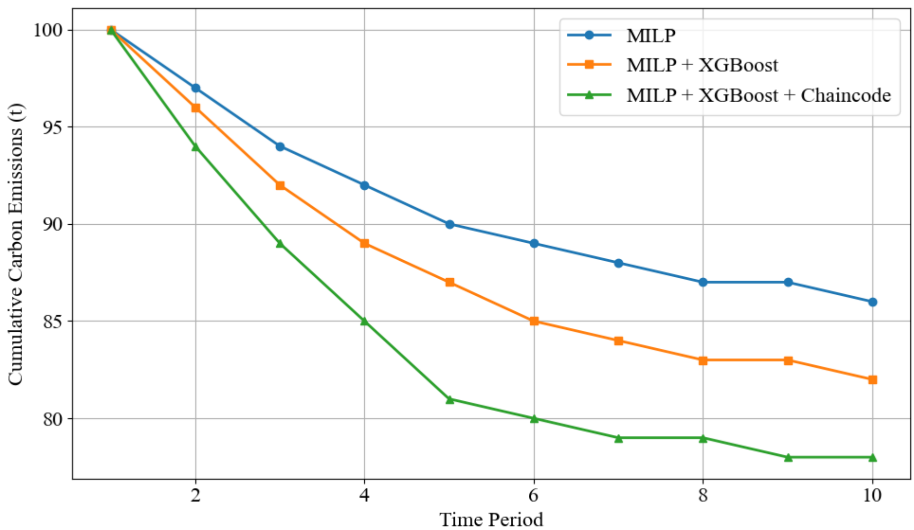

The differences in carbon emission paths among the three groups of mechanisms are mainly reflected in changes in cumulative emission levels and in the downward trend of the paths. The basic MILP model's cumulative carbon emissions drop to 86 tons in the 10th cycle. The overall decline is limited, and the rate of emission reduction between weeks is slow, indicating a lag in scheduling optimisation's response to marginal emission-reduction pressure. After introducing XGBoost, the system's cumulative emissions drop to 85 tons by the sixth cycle. The downward curve is steeper, and the adaptability of resource allocation to load changes is improved, leading to faster convergence in the emission path. After further integration of the chain code mechanism, the system's cumulative emissions have dropped to 85 tons in the fourth cycle, the emission decline rate has accelerated, the curve has become smoother, and the enhanced consistency of carbon data transmission has enabled the emission responsibility mapping to keep pace with resource adjustments, reducing the lag effect of emission control. The integration of multiple mechanisms effectively improves the dynamic efficiency of the system's carbon-emission-reduction path, helping increase the speed of achieving emission-reduction targets and the smoothness of operation.

6 Conclusion

This paper focuses on the problem of high marginal costs of reducing emissions in regional energy systems under carbon quota constraints. It constructs a multi-link digital scheduling framework that integrates MILP, XGBoost load forecasting, and the

Hyperledger Fabric chaincode mechanism. This paper integrates the resource-allocation logic for power generation, transmission, and distribution, as well as for terminal energy-consumption nodes, into the MILP model. It introduces carbon emission factors, a conversion efficiency matrix, and node energy balance constraints to optimise unit marginal emission-reduction cost under multi-node collaboration in the supply chain. At the data level, a regional load-forecasting model was built using the XGBoost algorithm. Based on four types of input features, namely historical load, electricity price, meteorology, and industrial activity intensity, the prediction accuracy and stability were significantly improved, with the lowest MAE being 8.1MW and the lowest RMSE being 11.4 MW. The chain code mechanism enables full-chain data encryption and storage, and quantifies node responsibilities in carbon information governance. The carbon data consistency ratio has improved to 0.963, and the Pearson coefficient is 0.976, significantly enhancing the transparency and credibility of carbon emission information. Multiple rounds of comparative experiments show that when the carbon quota is compressed to 50% of the system benchmark emissions, the unit marginal emission reduction cost of the model that fully integrates prediction and chain code mechanism in this paper is reduced from 278 yuan/ton to 245 yuan/ton, compared with the MILP model alone. The resource allocation efficiency and carbon responsibility structure are significantly optimised. The method in this paper provides a systematic, dynamic, and traceable technical path for the digital economy to empower the low-carbon transformation of regional energy systems from the perspective of the supply chain, effectively alleviating the problems of resource mismatch and information asymmetry under high-carbon constraints, and helping to build an efficient, transparent, and low-cost regional energy emission reduction system.

Conflict of interest

All authors declare that they have no conflicts of interest.

References

Bacanin, N., Stoean, C., Zivkovic, M., Rakic, M., Strulak-Wojcikiewicz, R. and Stoean, R. (2023) 'On the benefits of using metaheuristics in the hyperparameter tuning of deep learning models for energy load forecasting', *Energies*, Vol. 16, No. 3, pp.1434–1454.

Coors, V. and Padsala, R. (2024) 'Urban digital twins empowering the energy transition: citizen-driven, sustainable urban transformation towards positive-energy districts', *The International Archives of the Photogrammetry, Remote Sensing and Spatial Information Sciences*, Vol. 48, pp.51–56.

Fu, S., Liu, J., Tian, J., Peng, J. and Wu, C. (2023) 'Impact of digital economy on energy supply chain efficiency: evidence from Chinese energy enterprises', *Energies*, Vol. 16, No. 1, pp.568–588.

Gu, Z., Mousa, S., Meng, D., Elkady, A.M. and Leong, L.W. (2025) 'Digitizing energy supply chains for enhanced resilience: Exploring the nexus between supply chain digitization, carbon neutrality, and natural resource extraction', *Energy Economics*, Vol. 142, p.108177.

Heeß, P., Rockstuhl, J., Korner, M.F. and Struker, J. (2024) 'Enhancing trust in global supply chains: conceptualizing digital product passports for a low-carbon hydrogen market', *Electronic Markets*, Vol. 34, No. 1, pp.10–29.

Jiang, X., Sun, L. and Wang, Y. (2024) 'Effects of interactions between technology spillovers and carbon transfers on carbon-emission-reduction decisions and coordination within supply chains', *Journal of Business and Industrial Marketing*, Vol. 39, No. 7, pp.1497–1512.

Kong, L., Jin, X., Xu, Y. and Xu, K. (2025) 'The impact of China's total carbon emission control policy on low carbon total factor productivity', *Industry and Innovatio*n, Vol. 32, No. 4, pp.449–475.

Laing, H., O'Malley, C., Browne, A., Rutherford, T., Baines, T., Moore, A. and Willis, M.J. (2022) 'Optimisation of energy usage and carbon emissions monitoring using MILP for an advanced anaerobic digester plant', *Energy*, Vol. 256, p.124577.

Lameh, M., Al-Mohannadi, D.M. and Linke, P. (2022) 'Minimum marginal abatement cost curves (Mini-MAC) for CO2 emissions reduction planning', *Clean Technologies and Environmental Policy*, Vol. 24, No. 1, pp.143–159.

Li, C., Li, G., Wang, K. and Han, B. (2022) 'A multi-energy load forecasting method based on parallel architecture CNN-GRU and transfer learning for data deficient integrated energy systems', *Energy*, Vol. 259, p.124967.

Li, J., Mao, T., Huang, G., Zhao, W. and Wang, T. (2023) 'Research on day-ahead optimal scheduling considering carbon emission allowance and carbon trading', *Sustainability*, Vol. 15, No. 7, pp.6108–6130.

Luo, S., Wang, B., Gao, Q., Wang, Y. and Pang, X. (2024) 'Stacking integration algorithm based on CNN-BiLSTM-attention with XGBoost for short-term electricity load forecasting', *Energy Reports*, Vol. 12, pp.2676–2689.

Mao, J., Zhang, G., Ling, Z., Yuan, D., Liu, M. and Xu, J. (2024) 'Potentials of mixed-integer linear programming (MILP)-based optimization for low-carbon hydrogen production and development pathways in China', *Energies*, Vol. 17, No. 7, pp.1694–1711.

Onukwulu, E.C., Agho, M.O. and Eyo-Udo, N.L. (2021) 'Framework for sustainable supply chain practices to reduce carbon footprint in energy', *Open Access Research Journal of Science and Technology*, Vol. 1, No. 2, pp.12–34.

Pallikodathan, S., Man, H.C., Ghazi, T.I.M., Sulaiman, A., Nagarajoo, G. and Shukery, M.F. (2025) 'Minimizing carbon dioxide (CO2) emissions of POME treatment system using MILP model', *Processes*, Vol. 13, No. 2, p.583.

Shahbaz, M., Wang, J., Dong, K. and Zhao, J. (2022) 'The impact of digital economy on energy transition across the globe: the mediating role of government governance', *Renewable and Sustainable Energy Reviews*, Vol. 166, p.112620.

Shan-Shan, Y., Hao, G., Xiu, Y. and Zheng, L. (2023) 'Consideration and prospect of total carbon emission control system under the double carbon target', *Advances in Climate Change Research*, Vol. 19, No. 2, pp.191–202.

Sheikh, M.F., Padmanabhan, R., Hadid, M. and Kerbache, L. (2025) 'Towards additive manufacturing enabled sustainable spare parts supply chain: a multi-objective MILP model for cost and carbon emissions minimization', *Procedia Computer Science*, Vol. 253, pp.952–963.

Slamersak, A., Kallis, G. and O'Neill, D.W. (2022) 'Energy requirements and carbon emissions for a low-carbon energy transition', *Nature Communications*, Vol. 13, No. 1, pp.6932–6946.

Stroher, T., Korner, M.F., Paetzold, F. and Struker, J. (2025) 'Bridging carbon data's organizational boundaries: toward automated data sharing in sustainable supply chains', *Electronic Markets*, Vol. 35, No. 1, pp.1–22.

Sun, H., Zou, H., Wen, J., Ke, W. and Kou, L. (2024) 'Optimal scheduling considering carbon capture and demand response under uncertain output scenarios for wind energy', *Sustainability*, Vol. 16, No. 3, pp.970–990.

Sun, Y., Jiang, J. and Zhang, X. (2024) 'Effective carbon cost constraints: unity of environmental effectiveness, cost effectiveness, and incentive effectiveness', *Bulletin of Chinese Academy of Sciences* (*Chinese Version*), Vol. 39, No. 8, pp.1365–1374.

Tang, W., Wang, B., Wang, F., Tian, Y. and Zou, Y. (2023) 'Operation optimization of regional integrated energy systems', *Energy Science and Engineering*, Vol. 11, No. 12, pp.4542–4556.

Wang, J. and Zhao, C. (2023) 'Reducing carbon footprint in a resilient supply chain: examining the critical influencing factors of process integration', *International Journal of Production Research*, Vol. 61, No. 18, pp.6197–6214.

Wang, J., Wang, B., Dong, K. and Dong, X. (2022) 'How does the digital economy improve high-quality energy development? The case of China', *Technological Forecasting and Social Change*, Vol. 184, p.121960.

Wang, Z., Zhang, Y., Li, N. and Zhang, J. (2026) 'Spatiotemporal patterns and drivers of carbon emissions from on-site wastewater treatment: evidence from a city-wide long-term network', *Environmental Research*, Vol. 296, p.123948.

Wu, F., Wang, S.Y. and Zhou, P. (2023) 'Marginal abatement cost of carbon dioxide emissions: the role of abatement options', *European Journal of Operational Research*, Vol. 310, No. 2, pp.891–901.

Xu, L., Jia, F., Lin, X. and Chen, L. (2023) 'The role of technology in supply chain decarbonisation: towards an integrated conceptual framework', *Supply Chain Management: An International Journal*, Vol. 28, No. 4, pp.803–824.

Yang, Y., Peng, C. and Qing-Kui, L. (2024) 'Modeling and analysis of supply chain with green product change', *Cyber-Physical Systems*, Vol. 10, No. 1, pp.84–103.

Zampou, E., Mourtos, I., Pramatari, K. and Seidel, S. (2022) 'A design theory for energy and carbon management systems in the supply chain', *Journal of the Association for Information Systems*, Vol. 23, No. 1, pp.329–371.

Zhang, A. and Seuring, S. (2024) 'Digital product passport for sustainable and circular supply chain management: a structured review of use cases', *International Journal of Logistics Research and Applications*, Vol. 27, No. 12, pp.2513–2540.

Zhang, Y., Leng, Y., Shang, N., Liang, Z., Shi, H. and Luo, G. (2024) 'Bi-level optimal scheduling of power system considering carbon demand response and carbon trading', *Dianli Jianshe/ Electric Power Construction*, Vol. 45, No. 5, pp.94–104.

Zhang, Y., Xiao, Y., Shan, Q. and Li, T. (2023) 'Towards lower carbon emissions: a distributed energy management strategy-based multi-objective optimization for the seaport integrated energy system', *Journal of Marine Science and Engineering*, Vol. 11, No. 3, pp.681–700.

Zhang, Y., Zhang, P., Du, S. and Dong, H. (2024) 'Economic optimal scheduling of integrated energy system considering wind–solar uncertainty and power to gas and carbon capture and storage', *Energies*, Vol. 17, No. 11, pp.2770–2795.